Journal of Controlled Release 366 (2024) 746–760

Contents lists available at ScienceDirect

Journal of Controlled Release

journal homepage: www.elsevier.com/locate/jconrel

Tunable rigidity of PLGA shell-lipid core nanoparticles for enhanced pulmonary siRNA delivery in 2D and 3D lung cancer cell models

Hezhi Wang [a], Ye Yuan [a], Lu Qin [a], Mengmeng Yue [a], Jingwen Xue [a], Zhixiang Cui [a], Xuanguang Zhan [a], Jiayi Gai [a], Xin Zhang [a,b], Jian Guan [a,b], Shirui Mao [a,b,*]

[a] School of Pharmacy, Shenyang Key Laboratory of Intelligent Mucosal Drug Delivery Systems, Shenyang Pharmaceutical University, Shenyang 110016, China
[b] Joint International Research Laboratory of Intelligent Drug Delivery Systems, Ministry of Education, China

ARTICLE INFO

Keywords:
siRNA
Pulmonary delivery
Microfluidics
Hybrid nanoparticles
Cationic liposomes
Tumor penetration

ABSTRACT

Faced with the threat of lung cancer-related deaths worldwide, small interfering RNA (siRNA) can silence tumor related messenger RNA (mRNA) to tackle the issue of drug resistance with enhanced anti-tumor effects. However, how to increase lung tumor targeting and penetration with enhanced gene silencing are the issues to be addressed. Thus, the objective of this study is to explore the feasibility of designing non-viral siRNA vectors for enhanced lung tumor therapy *via* inhalation. Here, shell-core based polymer-lipid hybrid nanoparticles (HNPs) were prepared *via* microfluidics by coating PLGA on siRNA-loaded cationic liposomes (Lipoplexes). Transmission electron microscopy and energy dispersive spectroscopy study demonstrated that HNP consists of a PLGA shell and a lipid core. Atomic force microscopy study indicated that the rigidity of HNPs could be well tuned by changing thickness of the PLGA shell. The designed HNPs were muco-inert with increased stability in mucus and BALF, good safety, enhanced mucus penetration and cellular uptake. Crucially, HNP1 with the thinnest PLGA shell exhibited superior transfection efficiency (84.83%) in A549 cells, which was comparable to that of lipoplexes and Lipofectamine 2000, and its tumor permeability was 1.88 times that of lipoplexes in A549-3T3 tumor spheroids. After internalization of the HNPs, not only endosomal escape but also lysosomal exocytosis was observed. The transfection efficiency of HNP1 (39.33%) was 2.26 times that of lipoplexes in A549-3T3 tumor spheroids. Moreover, HNPs exhibited excellent stability during nebulization *via* soft mist inhaler. In conclusion, our study reveals the great potential of HNP1 in siRNA delivery for lung cancer therapy *via* inhalation.

1. Introduction

Lung cancer is one of the most common malignant tumors in the world. Non-small cell lung cancer (NSCLC) accounts for approximately 80–85% of all lung cancers, and about 80% of patients are already in the later period (stage III or IV) at the time of diagnosis [1]. Although chemotherapy and radiation therapy for advanced NSCLC patients have been relatively standardized, and the development of precision medicine has promoted the application of small molecule inhibitors in targeted therapy, the prognosis in the past 40 years has still been poor, and the 5-year survival rate is very low (~16%) [2,3]. Tumors have different mutation level, while traditional treatments often overlook the specificity of tumors [4]. Moreover, the acquired and inherent resistance of tumors are major challenges in available therapies, therefore there is an urgent need to develop novel treatments to address these issues [3].

With the outbreak of COVID-19, gene therapy has received great attention. RNA (Ribonucleic acid) therapy has the advantage of high specificity and a wide range of targets [4]. Currently, multiple targets have been identified in NSCLC patients, including epidermal growth factor receptor (EGFR), vascular endothelial growth factor (VEGF), and Kirsten rat sarcoma viral oncogene homolog (KRAS), *etc* [3]. Gene inhibition therapy can be applied in above targets. Small interfering RNA (siRNA) (~13 kDa) is generally a double-stranded RNA with a length of 21 to 23 base pairs (bp) [5,6]. Based on the characteristics of targets, the sequence of siRNA can be designed to achieve highly specific targeted therapy. When siRNA is delivered to the cytoplasm of lung cancer cells, it can produce gene silencing in the tumor related messenger RNA (mRNA), thereby inhibiting cancer cell proliferation, preventing tumor metastasis, and inducing cancer cell apoptosis [7].

However, despite of the fact that siRNA has great potential in the treatment of lung cancer, it is unstable and easily degraded by RNA enzymes. Therefore, it is absolutely essential to develop safe and

* Corresponding author at: School of Pharmacy, Shenyang Pharmaceutical University, 103 Wenhua Road, Shenyang 110016, China.
E-mail address: maoshirui@syphu.edu.cn (S. Mao).

https://doi.org/10.1016/j.jconrel.2024.01.029
Received 19 October 2023; Received in revised form 12 January 2024; Accepted 15 January 2024
Available online 20 January 2024

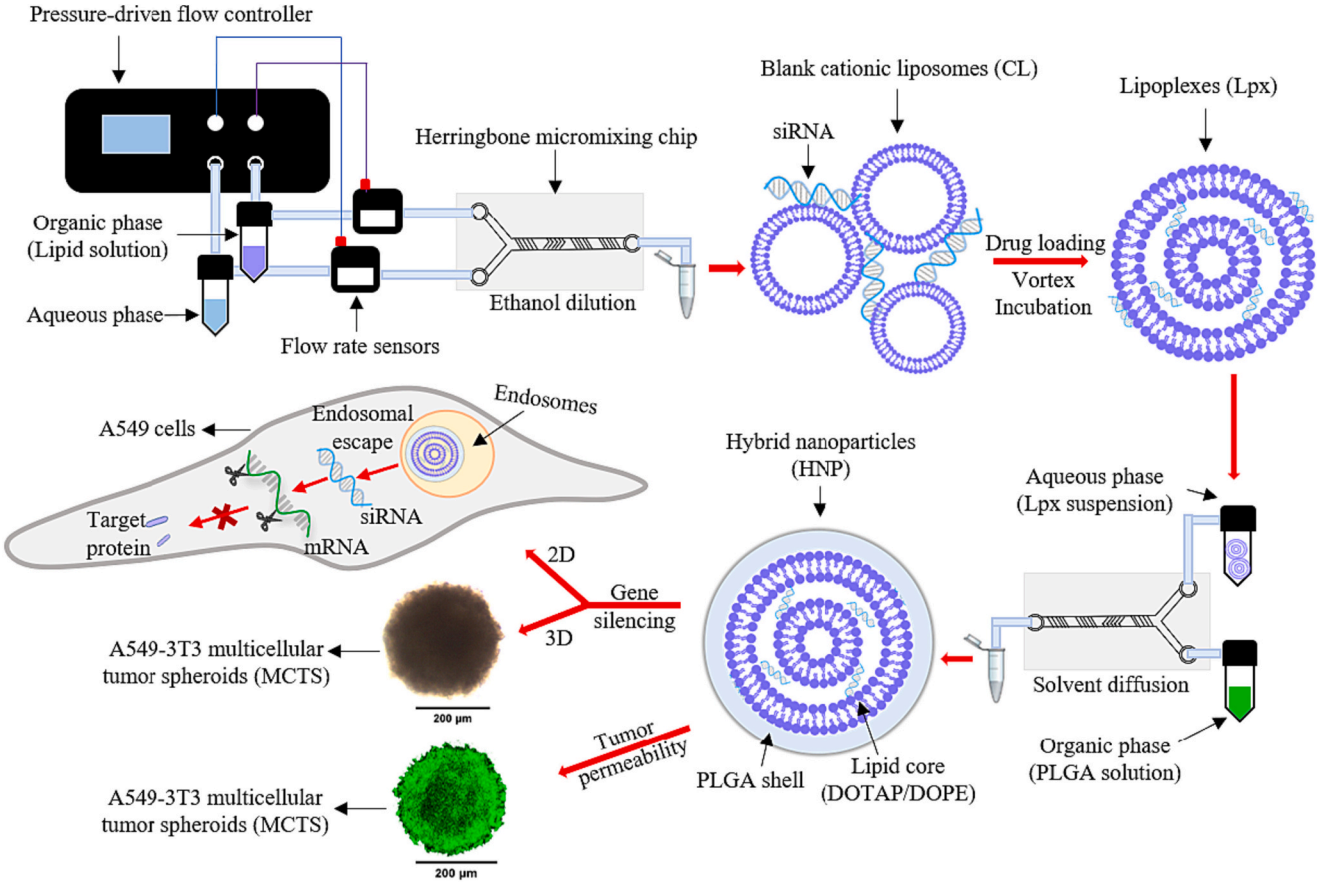

Fig. 1. Schematic of the setup for microfluidic preparation of cationic liposomes (CL), lipoplexes (Lpx), and hybrid nanoparticles (HNPs) *via* herringbone micromixing chip, as well as main studies, including gene silencing in both 2D- and 3D-cultured cells and tumor permeability in A549-3T3 tumor spheroids.

effective vectors to protect naked siRNA. For lung cancer therapy, pulmonary administration is a superior route while it can achieve high local concentration of anticancer drugs with reduced drug dose and systemic exposure, thus reduced toxicity [8,9]. However, in addition to increased local deposition, inhalable particles must be able to penetrate through the mucus layer and prevent being cleaned by cilia, as well as avoid being phagocytized by macrophages [10]. In addition to the extracellular barrier, it is also necessary to overcome the intracellular barrier by effectively escaping endo/lysosomes after tumor penetration [11]. Therefore, an ideal pulmonary siRNA delivery system for lung cancer therapy ought to satisfy the following requirements: (1) siRNA is efficiently encapsulated in vectors; (2) Inhalable vectors need to overcome the challenges of pulmonary delivery; (3) Vectors must penetrate into the deeper tumor; (4) siRNA must escape from the endo/lysosomes before being degraded.

In the widely reported gene delivery systems, non-viral vectors have low immunogenicity and are easy to design and synthesize compared to viral vectors [12]. Especially, cationic liposomes (CL) have the advantages of high *in vitro* transfection efficiency, great loading capacity, structural flexibility, and ease of large-scale production [13]. However, the high surface charge of CL leads to severe cytotoxicity, and it also has potential adverse interaction with negatively charged surface of lung cells [14]. Furthermore, CL is unstable in the pulmonary microenvironment and has poor mucus permeability, which makes CL unfavorable for pulmonary delivery [15]. Moreover, the poor tumor permeability of CL makes it unsuitable for the treatment of lung cancer [16]. Based on the above issues, our hypothesis is that by applying CL to efficiently compress and protect siRNA, and meanwhile using negatively charged and biodegradable Poly (D, L-lactic-*co*-glycolic acid) (PLGA) as coating material to cover the high positive surface charge of CL, not only improved safety and stability of CL, but also tunable rigidity as required for mucus and tumor penetration can be achieved after lung delivery.

Therefore, the objective of this paper is to develop safe and effective non-viral vectors suitable for lung cancer therapy *via* pulmonary siRNA delivery. First of all, blank CL was prepared using microfluidic method. Then, siRNA-loaded CL was obtained by two-step method. Subsequently, polymer-lipid hybrid nanoparticles (HNPs) were obtained by utilizing the high mixing and solvent diffusion of microfluidic technology. Next, multiple techniques (Surface potential measurement, transmission electron microscopy, and energy dispersive spectroscopy) were applied to elucidate the shell-core structure of HNPs. Moreover, influence of PLGA to total lipids weight ratios on the rigidity of HNPs was investigated *via* atomic force microscopy. The stability of different HNPs in pulmonary microenvironment, mucus permeability, cytotoxicity, and cellular uptake were also investigated. Crucially, the transfection efficiency in both 2D- and 3D-cultured cells and tumor permeability of different HNPs in A549-3T3 tumor spheroids were explored (Fig. 1). For pulmonary siRNA delivery, stability of the different HNPs was investigated after nebulization *via* soft mist inhaler.

2. Materials and methods

2.1. Materials

DOTAP (1,2-Dioleoyl-3-trimethylammonium-propane) and DOPE (1,2-dioleoyl-sn-glycero-3-phosphoethanolamine) were obtained from A.V.T. Pharmaceutical Co., Ltd. (Shanghai, China). PLGA (Resomer® RG 503H, lactide:glycolide 50:50, Mw 24,000–38,000 Da) was purchased

from Evonik Industries (Germany). TBE buffer, Tris (hydroxymethyl) aminomethane, RNA loading buffer (5×), and DEPC-treated water were obtained from Solarbio Biotechnology Co., Ltd. (Beijing, China). GelRed® was purchased from Biotium (California, USA). RiboGreen was obtained from Maokang Biotechnology Co., Ltd. (Shanghai, China). Fetal bovine serum (FBS) was obtained from Biological Industries (Israel). Ham's F-12 K medium was purchased from Procell Life Science Technology Co., Ltd. (Wuhan, China). Cell Counting Kit-8 (CCK-8), High Glucose Dulbecco's Modified Eagle Medium (DMEM), Optimal-Minimal Essential Medium (Opti-MEM), trypsin, RNase-free normal saline, 4′,6-Diamidino-2-phenylindole dihydrochloride (DAPI), and phosphate-buffered saline (PBS) were obtained from Meilun Biotechnology Co., Ltd. (Dalian, China). Ethanol, hydrochloric acid, and acetone were supplied by Yuwang Co., Ltd. (Shandong, China). Lipofectamine 2000 (Lipo2000) was purchased from Thermo Fisher Scientific (USA). Lyso-Tracker Green and Bio-Lumi™ II firefly luciferase assay kit (Bio-Lumi II) were obtained from Beyotime Biotechnology Co., Ltd. (Shanghai, China). Agarose and mucin 2 were purchased from Aladdin Biochemical Technology Co. Ltd. (Shanghai, China).

Firefly luciferase A549 cells were obtained from Yuchun Biology science and technology Co., Ltd. (Shanghai, China). BEAS-2B, RAW 264.7, and NIH-3T3 cells were provided by cell bank of Chinese Academy of Sciences (Shanghai, China). GL3 siRNA, scrambled/negative control (NC) siRNA, FAM NC siRNA, and Cy3 NC siRNA were purchased from Chengxin Biotechnology Co., Ltd. (Shanghai, China). GL3 siRNA sequences: sense (5′-3′) CUUACGCUGAGUACUUCGAdTdT, antisense (5′-3′) UCGAAGUACUCAGCGUAAGdTdT. Scrambled/NC siRNA sequences: sense (5′-3′) UUCUCCGAACGUGUCACGUdTdT, antisense (5′-3′) ACGUGACACGUUCGGAGAAdTdT.

2.2. Preparation of cationic liposomes and lipoplexes

Blank cationic liposomes were prepared *via* microfluidic method. The specific processes are as follows: DOTAP and DOPE were dissolved in anhydrous ethanol with a weight ratio of 1:3 to prepare a mixed lipid solution (5 mg/mL). Liposomes were prepared under different conditions, including aqueous media (Deionized water, Tris-HCl buffer (10 and 80 mM, pH 7.4), and 0.9% normal saline), flow rate ratio (FRR), and total flow rate (TFR), *via* Elveflow microfluidic system (Elveflow, France). The aqueous and organic phases were pushed by the OB1 pressure control device to the MFS4 and MFS5 flow sensors, followed by turbulent mixing of the two streams on a herringbone microfluidic chip, and the cationic liposome suspension was collected at the chip outlet. At room temperature, in order to remove ethanol, dialysis bags (Viskase MD34, Mw 8000–14,000 Da, USA) were used to obtain blank liposomes by dialysis with 1000 times the volume of deionized water relative to the suspension for 1 h. Afterwards, blank liposomes were mixed with equal volume siRNA solution in N/P ratios (Molar ratio of the DOTAP amine to the nucleotide) of 4:1, 6:1, and 8:1, vortex for 15 s, and incubated at room temperature for 30 min to obtain lipoplexes (Lpx).

2.3. Preparation of hybrid nanoparticles

Hybrid nanoparticles were prepared *via* microfluidic method. The specific processes are as follows: PLGA Resomer® RG 503H was dissolved in acetone as an organic phase. PVA0588 solution (Final concentration of 1.5%) was mixed with Lpx (N/P ratio of 6:1) in equal volume to form an aqueous phase. HNPs were prepared by rapidly diluting the organic phase using an aqueous phase (Lpx suspension) *via* Elveflow microfluidic system (Elveflow, France). The fixed conditions during the preparation process include FRR of 4:1 (*i.e.,* volume ratio of Lpx in PVA solution to PLGA in acetone is 4:1), TFR of 6.25 mL/min, different weight ratios of PLGA to total lipid (1:1, 2:1, and 3:1). At room temperature, dialysis bags (Mw 8000–14,000 Da) were used to remove acetone by dialysis with 1000 times the volume of deionized water relative to the HNPs suspension for 1 h. HNP suspension was filtered through a microporous membrane (0.8 μm) to remove PLGA precipitation. The HNPs suspension was placed in an ultrafiltration tube (Merck Millipore 50 kDa, USA) for centrifugation (1500 rpm) to remove most of PVA solution and concentrate the suspension.

2.4. Gel electrophoresis

The binding ability between CL and siRNA was investigated by gel retardation assay. Lpx (N/P ratios of 4:1, 6:1, and 8:1) were mixed with Triton X-100 (Final concentration of 1.25% (v/v)), vortex for 15 s, and incubated at room temperature for 15 min. As control, 10 μL RNA loading buffer (5×) was added into 40 μL Lpx. The complexes were loaded into an 2% (w/v) agarose gel stained with GelRed (10,000×). Gel electrophoresis (Tanon HE-120 and EPS-600, China) was run in TBE buffer at 100 V for 30 min. Gel strips were observed under UV irradiation *via* gel imager (Sagecreation ChampGel 5000 Plus, China). siRNA-loaded HNPs and Triton X-100 (Final concentration of 1.25% and 5% (v/v)) were rapidly mixed by vortexing, and the electrophoresis was performed as described above.

2.5. Determination of particle size and zeta potential

The intensity diameter and polydispersity index (PDI) of CL, Lpx, and HNPs were measured by dynamic light scattering (DLS) and Zeta potential was measured by Laser Doppler Electrophoresis *via* Zetasizer Nano ZS90 (Malvern Panalytical, UK). The temperature was 25 °C and the scattering angle was 90°. Each sample was measured three times.

2.6. Measurement of siRNA encapsulation efficiency

RiboGreen reagent (200×) was used to detect the content of siRNA in nanoparticles. Briefly, HNP suspension was centrifuged at 1500 rpm with ultrafiltration tubes (Merck Millipore 50 kDa, USA) to collect free siRNA solution. siRNA-loaded HNPs and 5% (v/v) Triton X-100 were rapidly mixed by vortex for 15 s, followed by incubation at room temperature for 15 min. 100 μL total siRNA solution or free siRNA solution and 100 μL RiboGreen reagent were added to the black 96 well plate. Fluorescence intensity was measured by microplate reader (SpectraMax M3, USA) with excitation wavelength (Ex) of 485 nm and emission wavelength (Em) of 528 nm. A standard curve ($R^2 = 0.9972$) was plotted to establish the correlation between siRNA and fluorescence intensity. The encapsulation efficiency (EE) of siRNA was calculated according to the following equation:

$$\mathrm{EE\%} = \frac{\text{Total siRNA} - \text{Nonencapsulated siRNA}}{\text{Total siRNA}} \times 100\%$$

2.7. Morphological observation

Morphology of nanoparticles was observed using transmission electron microscopy (TEM, JEM-1200EX, JEOL, Japan) at an accelerating voltage of 100 kV. Briefly, 10 μL sample was dropped onto a copper grid with carbon, and after 10 min, the excess liquid was suctioned by filter paper. 3% uranyl acetate was then dropped onto the copper grid and air dried at room temperature. ImageJ (USA) was used to measure thicknesses of the HNP1, HNP2, and HNP3 shells in TEM images. Each shell of HNP was analyzed 10 times in different directions. HNP2 with larger particle size was dipped on the copper grid mentioned above, and observed in the light and dark fields using scanning transmission electron microscopy (STEM) (FEI Tecnai G2 F30 S-TWIN, USA) at an accelerating voltage of 300 kV. Moreover, the surface elements of HNP2 were further characterized using energy dispersive spectroscopy (EDS) (Oxford Instruments XPLORE, UK) for mapping analysis.

2.8. Rigidity determination

Rigidity of CL and different HNPs were detected *via* measuring their Young's modulus by atomic force microscopy (Bruker Dimension ICON, Germany) in PeakForce QNM imaging mode. Briefly, suspension of the nanoparticles was dropped onto the surface of mica and air-dried at room temperature for 1 h. The samples were imaged with a scan rate of 1 Hz. A cantilever with a deflection sensitivity of 50.471 nm/V and a tip with a spring constant of 0.65 N/m were used. Young's modulus of each nanoparticle was analyzed by Nanoscope Analysis 1.7 (Bruker, Germany).

2.9. Mucus stability and mucus permeation study

The changes in particle size after co-incubation of nanoparticles with mucin were used to evaluate their stability upon contact with mucus. The details are as follows: mucin type 2 (From porcine stomach) powder was dispersed in water (0.08% w/v) and stirred overnight. The dispersion was centrifuged at 5000 rpm for 20 min to collect the mucin-containing supernatant [17,18]. Afterwards, 300 μL Lpx and HNPs were incubated with 1 mL mucin solution in air-bath oscillator (Shanghai Boxun, China) for 1, 3, and 6 h (37 °C, 100 rpm), followed by the measurement of particle size.

Transwell® based artificial mucus model was used to investigate the mucus permeability of Lpx and HNPs [15,17,18]. The specific process was as follows: Cy3 siRNA was diluted with PBS, and then the fluorescence intensity of Cy3 siRNA was measured by microplate reader (SpectraMax M3, USA) with excitation wavelength (Ex) of 550 nm and emission wavelength (Em) of 570 nm. Subsequently, a standard curve ($R^2 = 0.9939$) was plotted for the correlation between Cy3 siRNA and fluorescence intensity. The artificial mucus was prepared as previously described [18]. 200 μL artificial mucus was added to the upper chambers of Transwell-24 reservoir plate (Pore size: 5 μm), followed by the addition of 300 μL PBS in lower chamber. The plate was placed in air-bath oscillator (37 °C, 100 rpm) for 1 h, and then PBS was removed, followed by the addition of 300 μL fresh PBS. 70 μL Lpx and HNPs were added to the top of artificial mucus. The plate was placed in air-bath oscillator (37 °C, standstill). After 1, 4, and 20 h, 300 μL PBS was taken out, and the content of Cy3 siRNA was measured. Permeation percentage (%) was calculated according to the following equation:

$$\text{Permeation percentage } (\%) = \frac{\text{content of Cy3 siRNA in lower chamber}}{\text{total content of Cy3 siRNA initially added in upper chamber}} \times 100\%$$

2.10. Stability of cationic liposomes, lipoplexes, and hybrid nanoparticles in BALF

To test the stability of siRNA-loaded nanoparticles in the lung environment, nanoparticles were co-incubated with bronchoalveolar lavage fluid (BALF). BALF was collected from Sprague-Dawley (SD) rats (8-week-old, 180–230 g, from Animal Center in Shenyang Pharmaceutical University), the experiments were performed with permission from the Institutional Animal Care and Use Committee (IACUC) of Shenyang Pharmaceutical University, and the specific process was as previously described [15]. Insoluble impurities in BALF were removed through microporous membrane (0.45 μm). Subsequently, Lpx and HNPs were mixed with BALF in equal volume and incubated at 37 °C for 1 h. The electrophoresis experiment was carried out as described above. Additionally, the mixture was incubated in air-bath oscillator (Shanghai Boxun, China) for 1, 2, and 4 h (37 °C, 100 rpm). By examining the intensity diameter, polydispersity index, and zeta potential of nanoparticles, stability of the nanoparticles in BALF was determined.

2.11. Cell viability assay

Cell viability was evaluated using the Cell Counting Kit-8 (CCK-8) method. A549 cells and BEAS-2B cells were cultured in Ham's F-12 K medium supplemented with 10% (v/v) Fetal bovine serum (FBS) and 1% (v/v) penicillin/streptomycin. A549 and BEAS-2B cells were seeded at a density of 5×10^3 cells per well in a 96-well plate and incubated for 24 h. The medium was replaced with fresh medium containing 10, 40, 70, 100, and 130 nM GL3-siRNA loaded Lpx and HNPs. After 24 h, 100 μL F-12 K medium containing 10 μL CCK-8 was added to each well. After 1 h, absorbance was detected at 450 nm *via* microplate reader (SpectraMax M3, USA). The non-transfected group was selected as the control group, and the absorbance of culture medium containing 10 μL CCK-8 was used as background value to calculate cell viability.

2.12. Cellular uptake study

Flow cytometry was used to investigate the internalization of Lpx and HNPs. The specific process was as follows: A549 and RAW 264.7 cells were seeded at a density of 1.5×10^5 cells per well in a 12-well plate containing 1 mL of complete Ham's F-12 K medium and DMEM, respectively. The medium was replaced with fresh medium containing 50 nM Cy3 siRNA loaded-Lpx and HNPs. After 4 h, the cells were washed 3 times with PBS, and 200 μL trypsin was added to each well. Eventually, the cells were re-dispersed with PBS, and the fluorescence intensity was measured by LSRII flow cytometer (BD Biosciences, USA).

2.13. Transfection of A549 cells

Firefly luciferase A549 cells were seeded at a density of 3.5×10^3 cells per well in a 96-well plate and incubated for 24 h. After the cells were washed 2 times with PBS, Opti-MEM containing scrambled/GL3 siRNA-loaded Lipo2000 (0.25 μL Lipo2000 per well), Lpx, and HNPs were added to each well with a final siRNA concentration of 50 nM. After 6 h, Opti-MEM was replaced with fresh complete F-12 K medium. The cells were further cultured for 48 h, and firefly luciferase assay kit was added to the well by equal volume. After 10 min, the luciferase activity was measured *via* chemiluminescence detector (Promega Glomax Multi+ Detection System, USA).

2.14. Lysosomal escape characterization

A549 cells were seeded at a density of 4×10^4 cells per well in a 12-well plate and incubated for 24 h. Opti-MEM containing Cy3 siRNA-loaded Lipo2000, Lpx, and HNPs were added to each well with a final siRNA concentration of 50 nM. After 4 or 8 h, the cells were washed twice with PBS, followed by the addition of 1 mL F-12 K medium containing Lyso-Tracker Green (70 nM). After 1 h, 4% paraformaldehyde was used to fix cells for 30 min. Next, DAPI was used to stain nucleus for 20 min. The cells were visualized *via* CLSM (Nikon C2 plus, Japan) at 20× magnification.

2.15. Penetration of nanoparticles in multicellular tumor spheroids

3D-cultured tumor spheroids of A549-3T3 cells were constructed to investigate the tumor permeability of Lpx and HNPs. The main contents are as follows: The mixtures of A549 (5×10^3 cells/well) and 3T3 cells (5×10^3 cells/well) were seeded in a 96-well plate containing complete

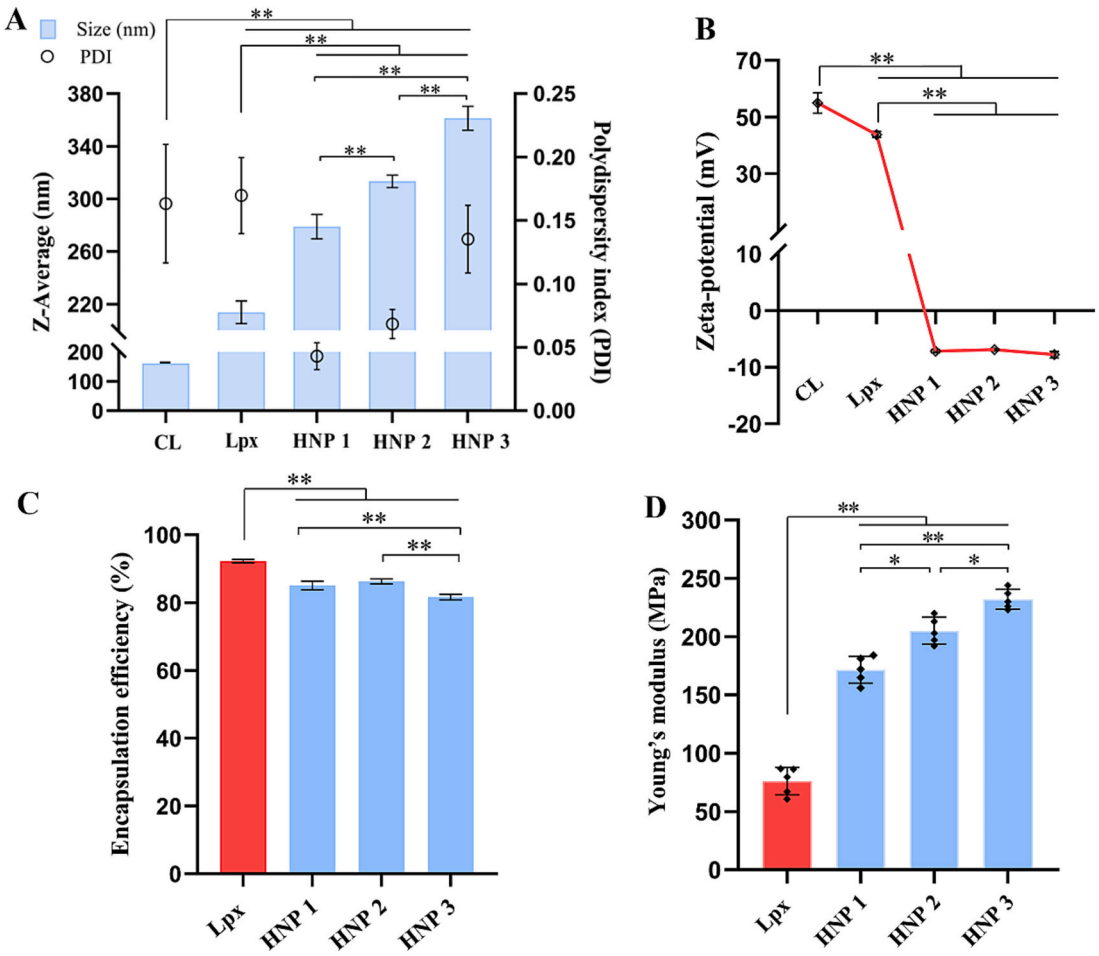

Fig. 2. (A) Particle size and size distribution of CL, Lpx, HNP1, HNP2, and HNP3. (B) Zeta-potential of CL, Lpx, and different HNPs. (C) Encapsulation efficiency of Lpx and different HNPs. Results denote mean ± SD ($n = 3$). (D) Young's modulus (MPa) of Lpx and different HNPs. Young's modulus of each nanoparticle was analyzed by Nanoscope Analysis 1.7 (Bruker, Germany). Results denote mean ± SD ($n = 5$). $p < 0.05$ (*), $p < 0.01$ (**).

Ham's F-12 K medium with 80 μL 2% sterile agarose. After 7 days, Opti-MEM containing FAM siRNA-loaded Lipo2000, Lpx, and HNPs were added to each well with a final siRNA concentration of 50 nM. After 6 h incubation, 4% paraformaldehyde was used to fix cells for 30 min. Subsequently, the tumor spheroids were observed using CLSM (Nikon C2 plus, Japan) at 10× magnification, followed by *Z*-axis scanning with a step of 20 μm.

2.16. Migration of nanoparticles in Transwell model

To confirm transcytosis of nanoparticles during the process of penetration in tumor spheroids, transwell model (Pore size: 1 μm) was used to observe the migration of different nanoparticles between A549 cells [19]. The specific process was as follows: A549 cells were seeded at a density of 1.5×10^5 cells per well in a 12-well plate and incubated for 12 h. The medium was replaced with fresh medium containing 50 nM FAM-siRNA loaded Lpx and HNP with PLGA to total lipids weight ratio of 1:1. After 4 h incubation, the cells were washed 3 times with PBS, and 200 μL trypsin was added to each well. 500 μL Opti-MEM containing A549 cells ((A) With or (B) without nanoparticles) was added to the upper chamber of Transwell and incubated for 4 h. (A) The coverslips with cells in the lower chamber were removed. (B) The cells in the upper chamber were digested and inoculated into a 12-well plate, and the coverslips were removed after 3 h. Then, the coverslips with cells were fixed with paraformaldehyde and stained with DAPI. Eventually, the cells were visualized *via* CLSM (Nikon C2 plus, Japan) at 20× magnification.

2.17. Transfection of multicellular tumor spheroids

To investigate the gene silencing of Lpx and HNPs in tumor tissue, transfection assay was conducted. 3D-cultured tumor spheroids of firefly luciferase A549-3T3 cells were constructed to simulate the tumor tissue of lung cancer. After 7 days incubation, Opti-MEM containing scrambled/GL3 siRNA-loaded Lipo2000, Lpx, and HNPs were added to each well with a final siRNA concentration of 50 nM. After 6 h, Opti-MEM was replaced with fresh complete F-12 K medium. After the tumor spheroids were further cultured for 48 h, they were transferred to a new 96-well plate with 100 μL firefly luciferase assay kit per well. After shaking for 15 min until the tumor spheroids were completely lysed. Luciferase activity was measured *via* chemiluminescence detector (Promega Glomax Multi+ Detection System, USA).

2.18. Nebulization of nanoparticles

Soft mist inhaler (SMI, Respimat, Boehringer-Ingelheim, Germany) was used to nebulize blank CL, Lpx, and HNPs. In brief, different nanoparticles were added to the drug cartridge of SMI. After rotating lower part of the inhaler, the dose release button was pressed immediately to nebulize suspensions of the different nanoparticles. Repeat this process 40 times to collect enough droplets for analysis.

2.19. Statistical analysis

All data in this paper were presented as mean ± standard deviation

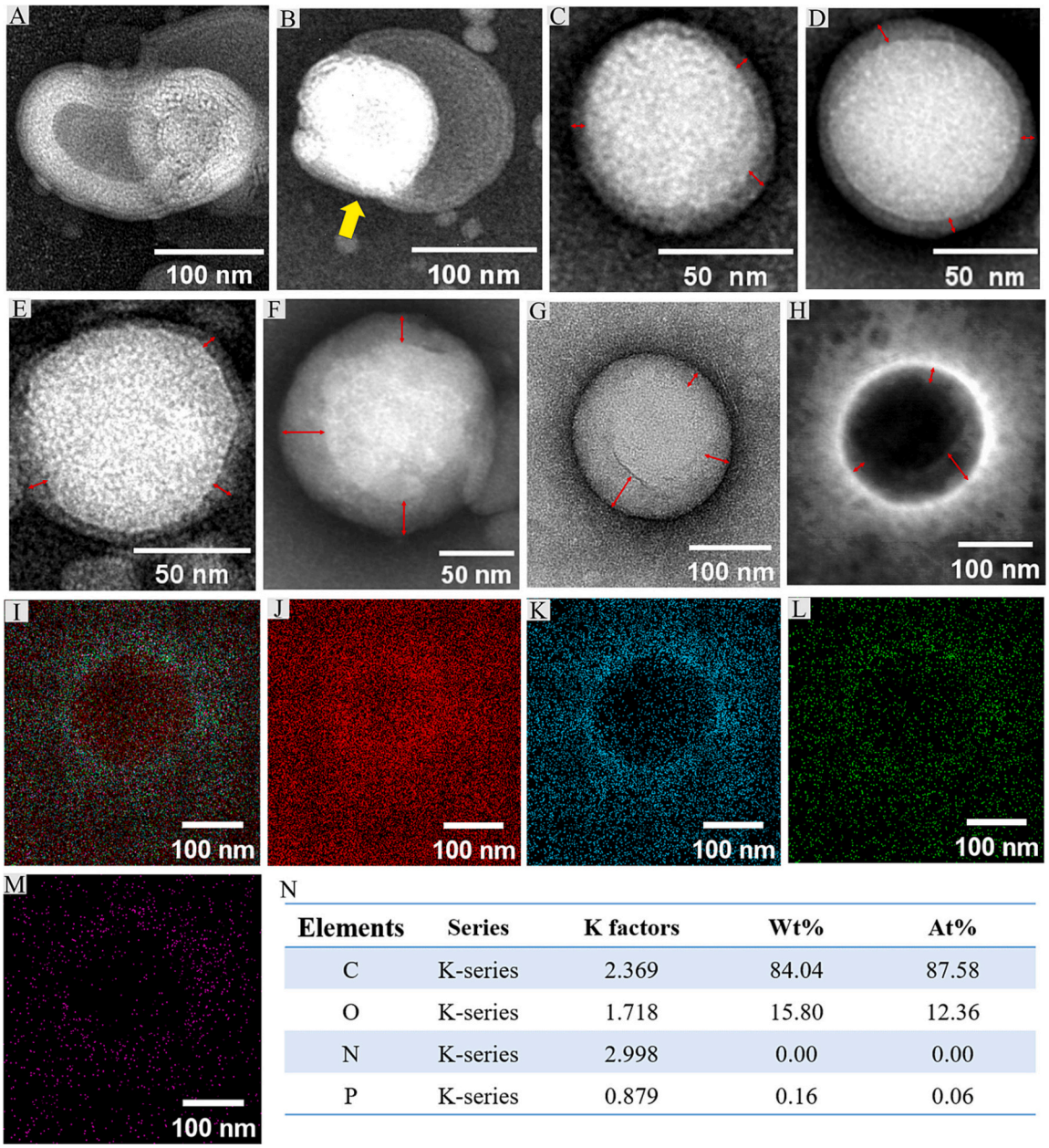

N

Elements	Series	K factors	Wt%	At%
C	K-series	2.369	84.04	87.58
O	K-series	1.718	15.80	12.36
N	K-series	2.998	0.00	0.00
P	K-series	0.879	0.16	0.06

Fig. 3. Transmission electron microscopy (TEM) images of (A, B) CL, (C) blank HNP1, GL3 siRNA-loaded (D) HNP1, (E) HNP2, and (F) HNP3. (G) Scanning transmission electron microscopy (STEM) image of GL3 siRNA-loaded HNP2. (H) High-angle annular dark field STEM image of GL3 siRNA-loaded HNP2. Energy dispersive spectroscopy (EDS) images of (I) elemental integration, (J) carbon, (K) oxygen, (L) nitrogen, and (M) phosphorus elements for the mapping analysis of HNP2. (N) Semi-quantitative analysis of elements, including weight percentage (Wt%) and atomic percentage (At%). Carbon and oxygen elements are provided by PLGA, DOTAP, DOPE, and siRNA. Nitrogen element is provided by DOTAP, DOPE, and siRNA. Phosphorus element is provided by DOPE and siRNA. The structure of shell is represented by red arrows. The CL with bleb structures is marked by yellow arrows. (For interpretation of the references to colour in this figure legend, the reader is referred to the web version of this article.)

(SD). Statistical analysis was performed by one-way ANOVA followed by Turkey's multiple comparison test using GraphPad Prism version 8.0.2 (GraphPad Software Inc., USA). Differences were considered as statistically significant at $p < 0.05$ (*).

3. Results and discussion

3.1. Preparation and characterization of blank cationic liposomes (CL) and lipoplexes (Lpx)

To achieve the complete compression of siRNA and ensure the subsequent efficient lysosomal escape, blank CL was first prepared as the core. Among the components of CL, 1,2-dioleoyl-3-trimethyllammonium propane (DOTAP) imparts positive charge to the liposomes, and DOTAP and 1,2-dioleoyl-sn-glycero-3-phosphoethanolamine (DOPE) jointly induce endosomal escape [16,20]. It has been reported that the fate of nanoparticles in the lung is influenced by their physicochemical properties (Particle size and surface potential). For instance, larger nanoparticles are easily phagocytosed by macrophages, leading to degradation of drugs and vectors [21]. The siRNA loading process of CL can lead to an increase in particle size. Therefore, it is necessary to ensure a smaller size of CL in the first step. Among the numerous preparation methods of CL, microfluidic-based ethanol injection technique has the advantages of excellent repeatability and easy scale-up

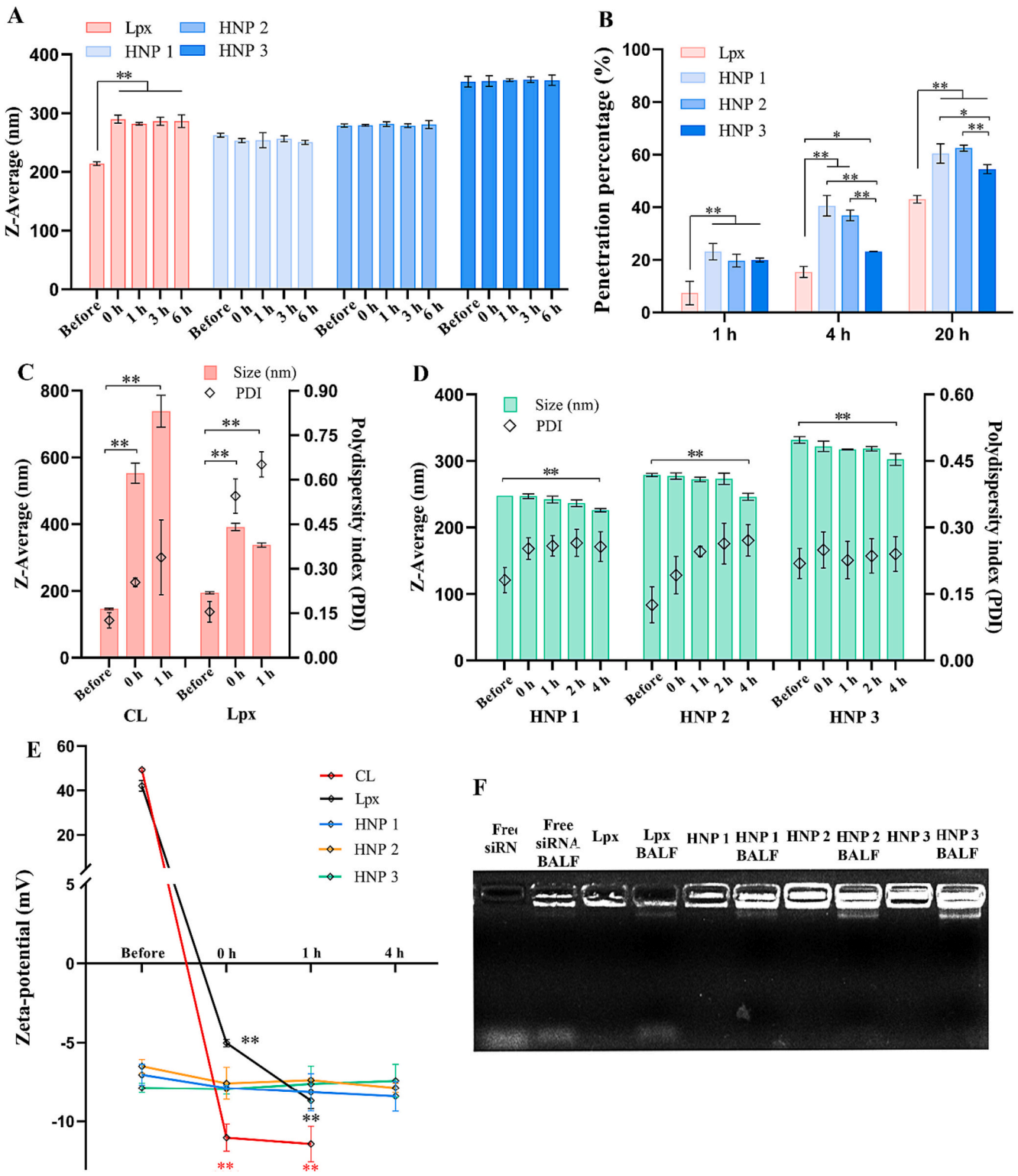

Fig. 4. (A) Particle size of Lpx, HNP1, HNP2, and HNP3 after incubated in mucin saturated solution for 6 h. (B) Permeation percentage of Cy3 siRNA-loaded Lpx and different HNPs in the artificial mucus. Particle size and size distribution of (C) CL, Lpx, and (D) different HNPs before and after incubation with rat bronchoalveolar lavage fluid (BALF) at specific time intervals. (E) Zeta-potential of CL, Lpx, and different HNPs before and after incubation with rat BALF. The results of all experimental groups were compared to those of the before BALF incubation groups. Results denote mean ± SD ($n = 3$). $p < 0.05$ (*), $p < 0.01$ (**). (F) siRNA leakage of Lpx and different HNPs in rat BALF at 1 h. The content of free siRNA in gel is ~95 ng.

production, and the physical properties of nanoparticles can be optimized through the precise control of microfluidic parameters [22,23]. To obtain blank liposomes with satisfied requirements, the effects of aqueous medium and microfluidic parameters (Flow rate ratio (FRR) and total flow rate (TFR)) on particle size of CL were investigated.

Firstly, the TFR of 2 mL/min and FRR (Aqueous phase: organic phase) of 3:1 were fixed to investigate the effects of aqueous media on the properties of CL, including deionized water, Tris buffer (10 mM, 80

mM), and normal saline. As shown in Fig.S1A, CL with uniform size can be obtained in all three aqueous media. The minimum CL size (~285 nm) and polydispersity index (PDI) (~0.15) were observed when the aqueous medium was normal saline (154 mM). Therefore, in subsequent experiments, normal saline was selected as the aqueous phase to further optimize the CL size by changing TFR. The effect of TFR on CL properties in the range of 2–6 mL/min was investigated under the conditions of fixed FRR (Aqueous phase: Organic phase) of 3:1 and normal saline as aqueous phase. The results revealed that the size of CL significantly decreased ($p < 0.01$) with TFR increased from 2 to 4 mL/min. Moreover, as TFR increased from 4 to 6 mL/min, the size of CL also significantly decreased ($p < 0.01$). The particle size of CL (~185 nm) and PDI (~0.13) were the smallest at TFR of 6 mL/min (Fig.S1B). Therefore, TFR of 6 mL/min was selected to further optimize the particle size of CL by changing the FRR. The effect of different FRR (Aqueous phase: Organic phase, 1:1, 3:1, and 5:1) on the properties of CL was investigated with the fixed TFR of 6 mL/min and normal saline as aqueous phase. The results showed that as FRR increased from 1:1 to 3:1, the particle size of CL significantly decreased ($p < 0.01$). In addition, the size of CL also significantly decreased ($p < 0.01$) as FRR increased from 3:1 to 5:1. Therefore, normal saline was chosen as the aqueous medium, and TFR of 6 mL/min and FRR of 5:1 were selected as the optimized microfluidic parameters. Finally, blank CL with size of ~152 nm, PDI of ~0.10, and Zeta potential of ~ + 55 mV was prepared (Fig.S1C).

After the preparation of blank CL, siRNA-loaded CL (Lipoplexes, Lpx) was obtained by directly mixing siRNA solution with blank CL and incubation. The effects of different N/P ratios (Molar ratio of the DOTAP amine to nucleotide, 4:1, 6:1 and 8:1) on drug loading were investigated by gel retardation assay. The group without Triton X-100 showed that there was bright band in the agarose gel at N/P ratio of 4:1, implying that the excess of unencapsulated siRNA moved to the positive pole under electric force, indicating siRNA was not fully bound to vectors. In contrast, there were no bands at N/P ratios of 6:1 and 8:1, implying that the siRNA was completely bound to vectors under these conditions. After 1.25% (v/v) Triton X-100 was added to CL suspension, bands were generated in the agarose gel, indicating Triton X-100 can damage the membrane of CL and lead to the leakage of siRNA (Fig.S1D). To increase drug loading while achieving complete binding between CL and siRNA, N/P ratio of 6:1 was selected for subsequent study. Eventually, Lpx with the particle size of ~210 nm and Zeta potential of ~ + 44 mV was prepared (Fig. 2A, B).

3.2. Preparation and characterization of lipid core-PLGA shell hybrid nanoparticles (HNPs)

To improve the safety, the high positive surface charge of CL was covered by coating with PLGA to form polymer-lipid nanoparticles *via* microfluidics. Here PLGA was chosen as the coating material not only due to its good biocompatibility but also its rigidity, which is required to enhance tumor penetration for lung cancer therapy. Thus, thickness of PLGA shell should be optimized while in addition to cover positive charge and enhance mucus/tumor permeability, it should be able to quickly rupture in the acidic environment of endo/lysosomes, allowing for the release of siRNA to exert its therapeutic effect. Therefore, first of all, the effect of PLGA to total lipids weight ratio (1:1, 2:1, and 3:1) on the properties of HNPs was investigated (Donated as HNP1, HNP2, HNP3 respectively). As shown in Fig. 2A, compared to Lpx, PLGA coating increased the size of HNPs significantly ($p < 0.01$) in a PLGA to total lipid ratio dependent manner, implying the formation of a core-shell structure. Also, the PDI of HNP1 and HNP2 significantly decreased compared to CL and Lpx, while no apparent change in PDI was observed for HNP3 attributed to its large size. Still, all the PDIs were <0.25, indicating uniform size distribution. As anticipated, PLGA coating indeed covered the positive charge of CL and Lpx and realized charge reversal to negative, no significant difference in surface charge between different HNP groups was found ($p > 0.05$) (Fig. 2B), implying HNP1 with the lowest proportion of PLGA is sufficient for the reversal of charges.

To test whether PLGA coating process influence the loading of siRNA, influence of PLGA to total lipids weight ratio on the encapsulation efficiency (EE) of HNPs was further investigated. As shown in Fig. 2C, compared to Lpx (~92%), the EE of HNPs decreased slightly, and the EE of HNP1 (~85%) and HNP2 (~86%) was higher than that of HNP 3 (~82%) ($p < 0.01$).

To further confirm whether HNP is the designed core-shell structure, morphology of the CL, blank HNP with PLGA to total lipids weight ratio of 1:1, siRNA-loaded HNP1, HNP2, HNP3 was observed *via* transmission electron microscopy (TEM). As shown in Fig. 3A, the lipid membrane and aqueous core of CL can be clearly observed. During the process of removing ethanol by dialysis, liposomes fused with each other to form bleb structures [24], including aqueous regions (Dim) and lipids enriched regions (Bright) (Fig. 3B, Fig.S2A). In contrast, a sharp core-shell structure with spherical shape and dense membrane was observed for HNPs, as marked by red arrows (Fig. 3C-F), and remarkably increased member thickness was noted for HNP3 (Fig. 3F). As shown in Fig. 3D-F, shell thickness of the HNP1, HNP2, and HNP3 was 4.76 ± 1.10 nm, 7.14 ± 1.28 nm, and 20.06 ± 4.16 nm, respectively, demonstrating the shell thickness increased with the increase of PLGA to total lipids weight ratio. Taking HNP2 as an example, the core-shell structure was further confirmed by scanning transmission electron microscopy (STEM) (Fig. 3G, H).

Moreover, to demonstrate the outer shell is mainly composed of PLGA, taking HNP2 as an example, energy dispersive spectroscopy (EDS) was applied to analyze the elements of HNP. Carbon and oxygen elements are provided by PLGA, DOTAP, DOPE, and siRNA. Nitrogen element is provided by DOTAP, DOPE, and siRNA. Phosphorus element is provided by DOPE and siRNA. As shown in Fig. 3I-M, after mapping analysis, carbon, oxygen, and lower ratio of phosphorus elements was observed in the enriched area corresponding to the outer shell of HNP. Further semi-quantitative calculation results showed that the weight percentage (Wt%) and atomic percentage (At%) of nitrogen elements were both 0% (Fig. 3N), with high ratio of carbon and oxygen components and limited phosphorus, while PLGA is composed only of carbon and oxygen elements, implying the shell does not contain DOTAP, the content of DOPE and siRNA is negligible. The above results indicated the shell is mainly composed of PLGA.

In addition, to test the hypothesis of tunable rigidity by PLGA coating, the Young's modulus of different nanoparticles was detected *via* atomic force microscopy (AFM). As shown in Fig. 2D, the Young's modulus of HNP1, HNP2, and HNP3 was 2.26, 2.70, 3.05 times that of Lpx ($p < 0.01$), demonstrating PLGA coating indeed has the capacity to tune rigidity of the nanoparticles, which provided the prerequisite for enhanced mucus and lung tumor penetration.

3.3. In vitro mucus stability and mucus penetration

For lung cancer therapy *via* inhalation, nanoparticles deposited in the airway must be stable, with robust size to penetrate through the mucus and get contact with the lung tumors, otherwise they will be cleared by the mucociliary clearance system, thereby hindering the uptake of non-viral vectors by target cells [11]. Thus, first of all, stability of the Lpx and HNPs in mucus was investigated. As shown in Fig. 4A, upon contact with mucus, particle size of the positively charged Lpx increased significantly ($p < 0.01$), indicating negatively charged mucins immediately adsorbed on the surface of Lpx, and the size increase is detrimental to mucus penetration. The size of Lpx did not change further within the followed 6 h ($p > 0.05$). In contrast, no significant change in particle size was observed for the three HNPs during 6 h incubation with mucus ($p > 0.05$), indicating PLGA coating increased the stability of HNPs in mucus. Their muco-inert property may be attributed to the near-neutral surface charge. The above results suggested that the coating strategy with PLGA effectively solved the problem of size

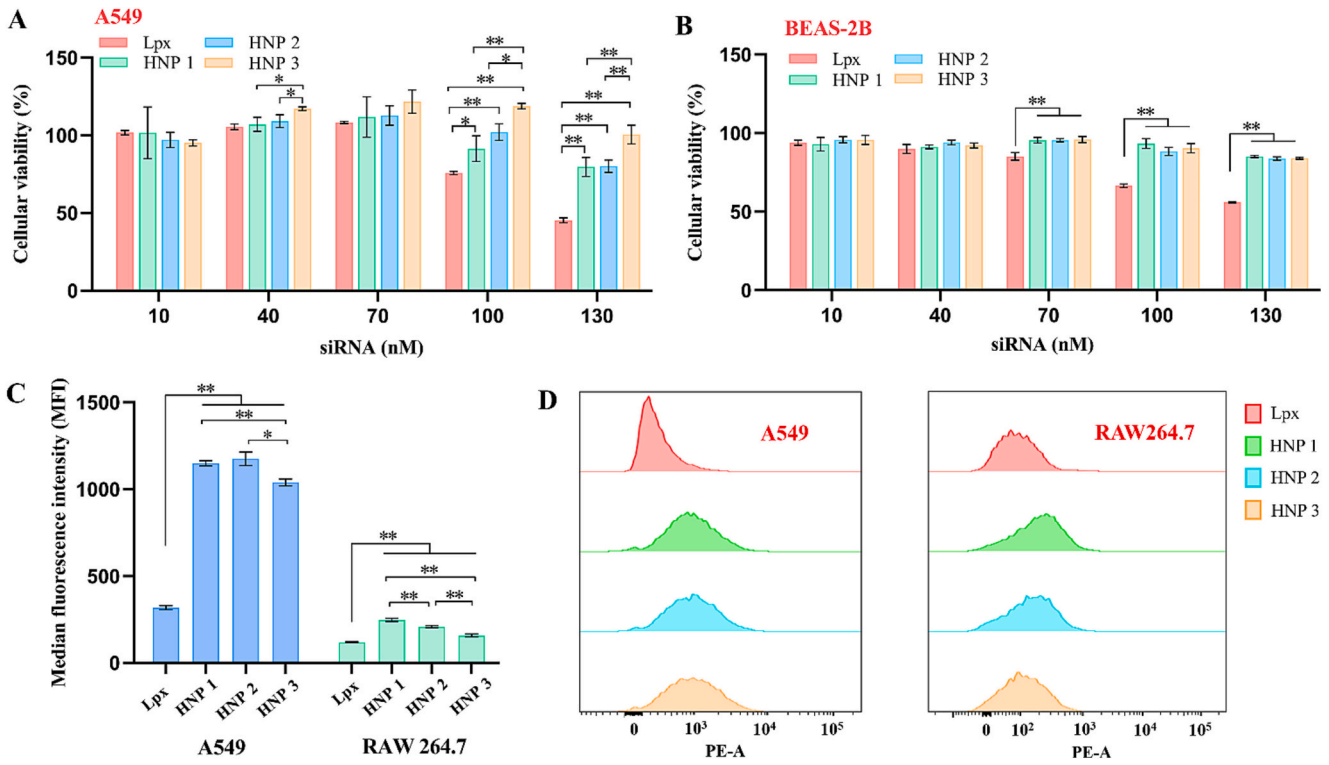

Fig. 5. Cellular viability of GL3 siRNA-loaded Lpx, HNP1, HNP2, and HNP3 in (A) A549 and (B) BEAS-2B cells. Concentration of GL3 siRNA ranges from 10 to 130 nM. (C) Cellular uptake of the different nanoparticles in A549 and RAW 264.7 cells at 4 h by flow cytometry. Mean fluorescence intensity (MFI) was analyzed by FlowJo (v10.8.1, USA). Results denote mean ± SD ($n = 3$). $p < 0.05$ (*), $p < 0.01$ (**). (D) Histograms of cellular uptake in A549 and RAW 264.7 cells at 4 h by flow cytometry. The concentration of Cy3 siRNA is 50 nM.

increase caused by the interaction between Lpx and mucin.

Thereafter, whether increased rigidity is beneficial to mucus penetration was further investigated. As shown in Fig. 4B, mucus permeability of both Lpx and different HNPs was time dependent, and as anticipated, all the HNPs presented enhanced mucus permeation compared to that of Lpx at 1, 4, and 20 h ($p < 0.05$). Regarding to the influence of PLGA modification ratio, no statistical difference among HNP1, HNP2 and HNP3 was found in permeation at 1 h. However, HNP3 presented decreased mucus permeation compared to HNP1 and HNP2 at 4 and 20 h ($p < 0.05$), while no statistical difference in mucus permeation was found between HNP1 and HNP2 in all the time points investigated ($p > 0.05$). These results are in good agreement with the above stability results in mucus. Airway mucus has a network architecture, with pore diameters ranging from tens to hundreds of nanometers [25]. The adsorption of negatively charged substances on the surface of Lpx leads to an increase in particle size, which may cause Lpx to be intercepted by the mucin network, ultimately resulting in an extension of the residence time of Lpx in the mucus [10]. In contrast, the neutral surface of HNPs can prevent interaction with negatively charged substances in artificial mucus, which is beneficial for particle diffusion. The decreased mucus permeation of HNP3 at 4 and 20 h, may be attributed to its largest particle size, which not only reducing its diffusion rate but also being easily intercepted [25].

3.4. In vitro stability in BALF

For pulmonary delivery, when inhalable particles deposited in the deep lung region, the pulmonary surfactant can potentially interact with drugs and vectors, even leading to their destruction. Therefore, to achieve siRNA delivery for lung tumor therapy, its stability in BALF must be guaranteed. As shown in Fig. 4C, CL or Lpx were not stable upon contact with bronchoalveolar lavage fluid (BALF), and their particle size increased immediately ($p < 0.01$) with surface charge reversal (Fig. 4E). Furthermore, both CL and Lpx could not be detected by dynamic light scattering at 2 h, indicating most CL and Lpx were destroyed. This may be due to electrostatic attraction between the positively charged blank CL or Lpx and negatively charged substances (*e.g.*, mucin and pulmonary surfactant proteins) in BALF, leading to the fusion of CL and aggregation of Lpx [15]. Gel electrophoresis analysis at 1 h (Fig. 4F) further indicated the poor stability of Lpx in BALF, with leakage of siRNA. In contrast, PLGA coating improved stability of HNPs significantly, no significant change in the particle size and surface charge of HNPs before and after mixing with BALF was found ($p > 0.05$) (Fig. 4D, E), despite of different PLGA coating ratio. Similarly, agarose gel analysis at 1 h further demonstrated that all the HNPs could protect siRNA from leakage in BALF (Fig. 4F). This study demonstrated that compared to Lpx, PLGA coated HNPs exhibited good stability in mucus and BALF, with enhanced mucus permeability, implying their potential as non-viral siRNA vectors for lung cancer therapy *via* inhalation.

3.5. In vitro cytotoxicity

In addition to poor stability in mucus and BALF, the high positive charge is also the barrier to prevent CL being used as a non-viral vector for pulmonary siRNA delivery. To test the feasibility of using PLGA coating to improve the safety of CL in the lung, A549 cell line was selected as cell model of human-type II alveolar epithelial cell and BEAS-2B cell line was chosen as cell model of normal human bronchial epithelial cell to investigate the cytotoxicity of Lpx and different HNPs. The recommended siRNA concentration for *in vitro* commercial non-viral transfection reagent-based gene silencing assay is generally 10–100 nM, so a concentration gradient of 10–130 nM was set for cell viability study. As shown in Fig. 5A, both Lpx and different HNPs exhibited high cell viability at concentrations of 10–70 nM in A549 cells. However, at high siRNA concentrations of 100 and 130 nM, the cell viability of Lpx was significantly reduced and it was only approximately

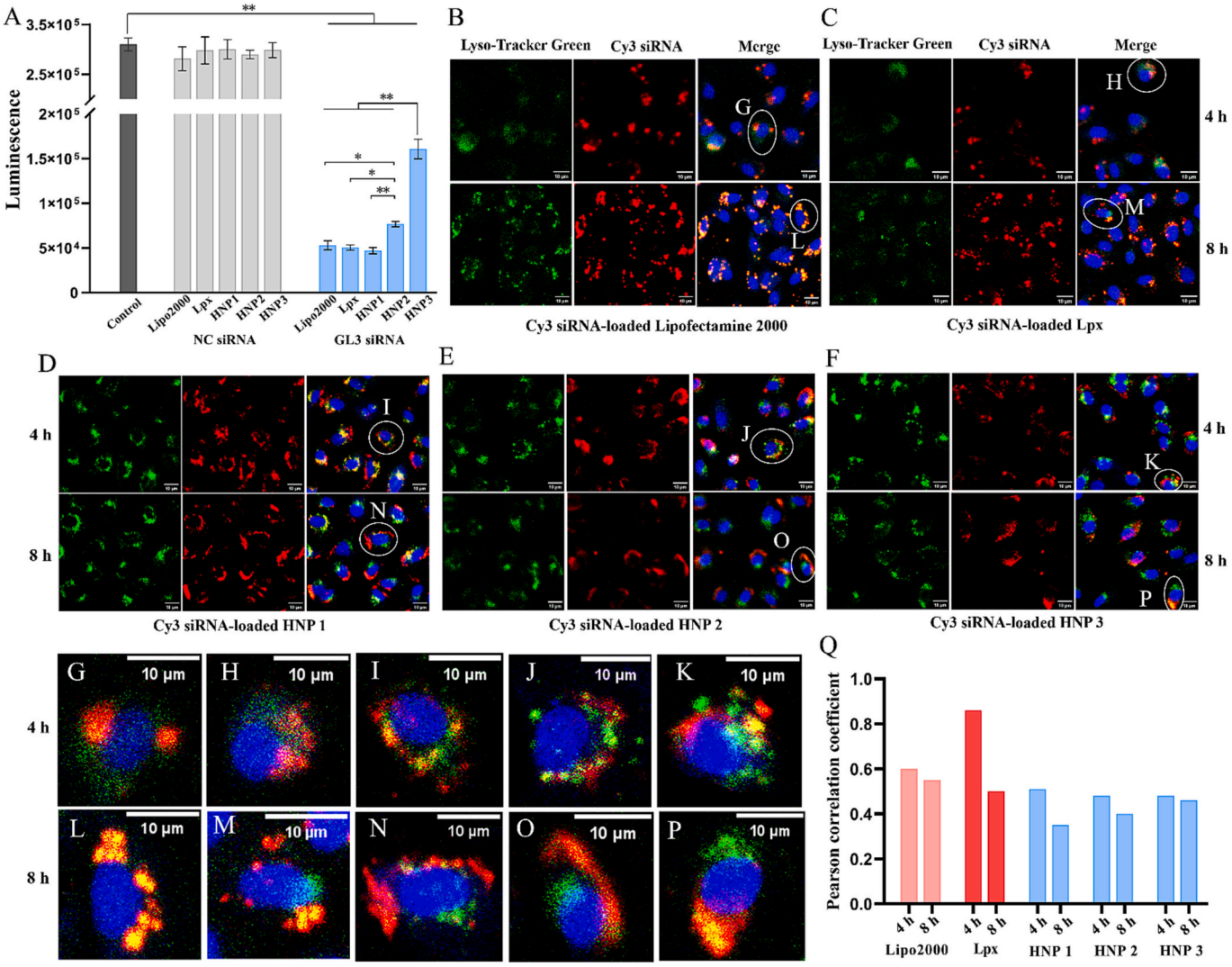

Fig. 6. (A) Luminescence of firefly luciferase A549 cells after 48 h of transfection with scrambled (NC)/GL3 siRNA-loaded Lipo2000, Lpx, HNP1, HNP2, and HNP3. The concentrations of both scrambled and GL3 siRNA are 50 nM. The results of all NC and experimental groups were compared to that of the blank control group. Results denote mean ± SD ($n = 3$). $p < 0.05$ (*), $p < 0.01$ (**). Confocal images of the endo/lysosomal escape of Cy3 siRNA-loaded (B) Lipo2000, (C) Lpx, (D) HNP1, (E) HNP2, and (F) HNP3 in A549 cells at 4 and 8 h. Local magnified images of the endosomal escape of (G) Lipo2000, (H) Lpx, (I) HNP1, (J) HNP2, and (K) HNP3 at 4 h (White circles in (B—F) respectively), as well as (L) Lipo2000, (M) Lpx, (N) HNP1, (O) HNP2, and (P) HNP3 at 8 h (White circles in (B—F) respectively). The blue fluorescence signal represents cell nucleus, red fluorescence represents Cy3 siRNA, and green fluorescence signal represents late endo/lysosomes. The concentration of Cy3 siRNA is 50 nM. The scale bar is 10 μm. (Q) Pearson correlation coefficient (PCC) (Above threshold) of the co-localized fluorescence regions of Cy3 siRNA (Red) and late endo/lysosomes (Green) in confocal images at 4 and 8 h. All cells in confocal images (8–18 cells) were analyzed using the Color2 function in ImageJ (USA). (For interpretation of the references to colour in this figure legend, the reader is referred to the web version of this article.)

50% compared to over 80% of HNP1 and HNP2, and no significant difference in cell viability between HNP1 and HNP2 was found ($p > 0.05$). The cell viability of HNP3 was the highest among all the groups ($p < 0.05$), possibly due to the thickest PLGA shell. Similarly, as shown in Fig. 5B, Lpx exhibited high cell viability at concentrations of 10–70 nM in BEAS-2B cells (Over 80%). However, at concentrations of 70–130 nM, cell viability of the Lpx was significantly lower than that of HNP1 HNP2, and HNP3 ($p < 0.01$). Contrarily, different HNPs showed over 80% cell viability in all siRNA concentrations. These results verified the PLGA shell enhanced the safety profile of Lpx during pulmonary delivery, as it shielded high positive surface charge of Lpx.

3.6. *In vitro* cellular uptake

After safe non-viral vectors being delivered to the lung, in addition to good mucus permeation and stability in BALF, they must be able to ingested by the target cells in order to further release siRNA and silence the target mRNA in cytoplasm. The quantitative results from flow cytometry demonstrated that after A549 cells were incubated with Cy3 siRNA-loaded nanoparticles for 4 h, cellular uptake of all the HNPs was ~3.3 times that of Lpx, but the cellular uptake of HNP3 was lower than that of HNP1 and HNP2 ($p < 0.05$) (Fig. 5C, D). Some researches proved that rigid nanoparticles exhibited enhanced cellular uptake compared to flexible nanoparticles [26–28]. Therefore, perhaps an appropriate increase in the rigidity of Lpx is beneficial for cellular uptake, but excessive rigidity of Lpx may reduce cellular uptake.

Also, in the deep lung there are a large amount of macrophages, nanoparticles need to escape the phagocytosis of alveolar macrophages in order to increase the chance of being ingested by target cells. Thus, influence of PLGA coating on the cellular uptake of nanoparticles in alveolar macrophages was further investigated. RAW 264.7 cell lines were selected as cell models of alveolar macrophages, and the cellular uptake of different nanoparticles was quantified by flow cytometry at 4 h. As shown in Fig. 5C, the fluorescence intensity of Lpx and HNPs in

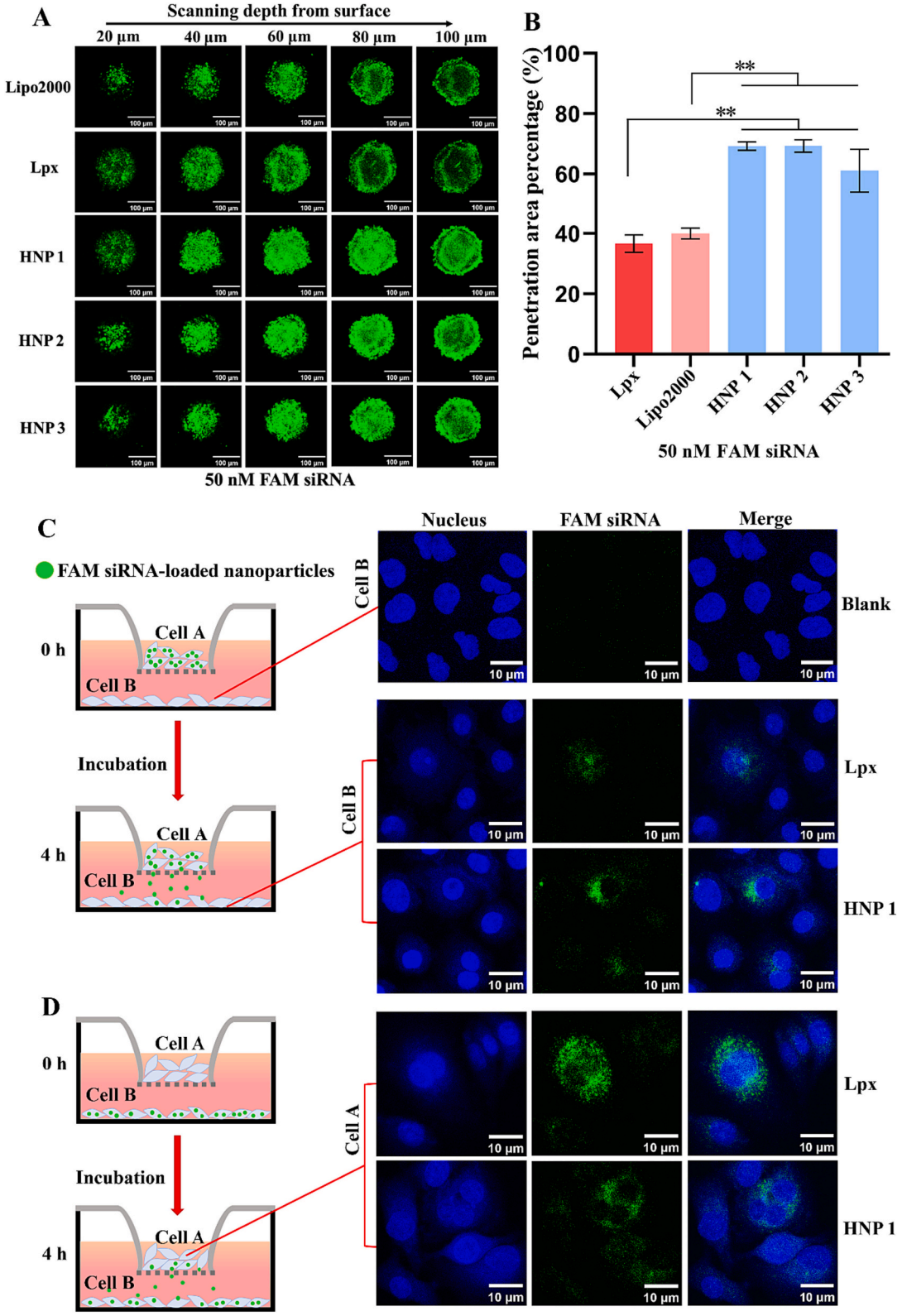

Fig. 7. (A) *Z*-Stack confocal images of 3D-cultured A549-3T3 multicellular tumor spheroids (MCTS) after incubation with FAM siRNA-loaded Lipo2000, Lpx, HNP1, HNP2, and HNP3 at 6 h. The surface of the MCTS is defined as 0 μm. The scale bar is 100 μm. (B) The penetration area percentage of different nanoparticles at the 100 μm depth sections of MCTS. By setting a unified threshold in Image J, the percentage of penetration area in the total tumor area is calculated. Results denote mean ± SD ($n = 3$). $p < 0.01$ (**). Left images represent Transwell based migration model. Right images: (C) Confocal images of blank cell B at 0 h and cell B in the lower chamber at 4 h. Cell A represents A549 cells that had pre-ingested the FAM siRNA-loaded Lpx or HNP1. Cell B represents blank A549 cells. (D) Confocal images of cell A in the upper chamber. Cell A represents blank A549 cells. Cell B represents A549 cells that had pre-ingested the FAM siRNA-loaded Lpx or HNP1. The concentration of FAM siRNA is 50 nM.

A549 cells was ~2.7 and ~ 5.5 times that of in RAW 264.7 cells, respectively, indicating RAW 264.7 had a lower uptake of Lpx and all the HNPs, which are beneficial for lung retention and tumor penetration. Moreover, it was also noted that macrophage uptake of HNP1, HNP2, and HNP3 was 2.1, 1.7, and 1.3 times that of Lpx, respectively. Our previous study found that liposomes with higher membrane fluidity displayed lower macrophage uptake [29]. Thus, the enhanced macrophage uptake of all the HNPs may be due to increase in their rigidity. These results revealed that HNPs were not favorable for macrophage uptake, so they were inclined to be taken by tumor cells.

3.7. In vitro gene silencing and endosomal escape in A549 cells

The above studies demonstrated that all the HNPs can well overcome the barriers in the lung with enhanced cellular uptake and good safety profile. However, after PLGA surface coating, whether the high transfection capacity of CL can still be maintained is a critical concern. The transfection efficiency will determine whether HNPs can be used as a promising candidate for pulmonary siRNA delivery. Thus, the transfection efficiency of different vectors was further investigated. Here, commercial transfection reagent Lipofectamine 2000 (Lipo2000), Lpx, and three HNPs were used to transfect firefly luciferase A549 cells, and luciferase activity was measured. The positive control groups are GL3 siRNA loaded-Lipo2000 and Lpx, and the negative control groups are scrambled siRNA loaded-nanoparticles. As shown in Fig. 6A, no significant difference in gene silencing between the blank control group and negative control groups was found ($p > 0.05$), indicating the nanoparticles had no non-specific effect on cell viability. Thus, luminescence was not affected by NC siRNA and different nanoparticles, and specific siRNA effects could be safely determined. Compared to the negative control group, Lipo2000, Lpx, and HNPs were all able to effectively produce gene silencing ($p < 0.01$). Among them, HNP1 produced the most significant gene silencing, and gene silencing gradually decreased as the weight ratio of PLGA to total lipids increased ($p < 0.01$). Notably, the gene silencing of HNP1 was similar to that of Lipo2000 and Lpx ($p > 0.05$), implying PLGA could maintain the high transfection efficiency of Lpx in 2D-cultured A549 cells. When the transfection efficiency of blank control group was set at 0%, the transfection efficiency of Lipo2000, Lpx, HNP1, HNP2, and HNP3 were 82.89 ± 1.34%, 83.71 ± 0.76%, 84.83 ± 0.92%, 75.24 ± 0.79%, and 48.19 ± 2.89%, respectively, demonstrating HNP1 owns not only good protection to siRNA but also comparable gene silencing capacity to Lpx. Compared to HNP1, the decreased gene silencing capacity of HNP2 and HNP3 might be explained by the increased thickness of PLGA shell, making it difficult for the shell to break in endo/lysosomes, thus affecting the release of siRNA and therefore reduced transfection efficiency.

To further confirm PLGA shell thickness is a critical parameter influencing endo/lysosomal escape of HNPs, endosomal escape of the Lipo2000, Lpx, and three HNPs were observed *via* CLSM. As shown in Fig. 6B-F, when the incubation time extended from 4 to 8 h, the red fluorescence of positive control group (Lipo2000 and Lpx) increased, indicating an increase in cellular uptake. Meanwhile, clear yellow co-localization regions were observed, indicating all the nanoparticles entered the endosomes after internalization. To observe the endosomal escape more clearly, the successful escape images of Lipo2000, Lpx, and three HNPs at 4 h (Fig. 6G-K) and 8 h (Fig. 6L-P) were locally magnified. The yellow co-localized region indicated that siRNA was trapped in endo/lysosomes, while the separated late endo/lysosomes (Green) and siRNA (Red) represented the occurrence of endosomal escape. Pearson correlation coefficient (PCC) was used to indicate the degree of co-localization, and the higher the degree of co-localization, the closer the value of coefficient to 1 [30]. As shown in Fig. 6Q, from 4 to 8 h, the co-localized areas of Lipo 2000, Lpx, and different HNPs decreased, suggesting that over time, siRNA escaped from the endosomes and entered the cytoplasm. Among different HNPs, PCC of HNP1 decreased from 0.51 to 0.35, implying its strongest ability of endo/lysosomal escape attributed to its thinner shell. Thus, to achieve high transfection efficiency by HNPs, a balance between stability of HNPs and rupture of PLGA shell in endo/lysosomes must be satisfied, in order to ensure the exposure of lipid core in endo/lysosomes after cellular uptake, and the exposed lipids, including DOTAP and DOPE, jointly trigger membrane fusion with endosomal membrane, resulting in efficient endosomal escape and release of siRNA [16,20].

3.8. Influence of PLGA shell thickness on the penetration of HNPs in multicellular tumor spheroids

After proving that HNPs have good stability in BALF, excellent mucus permeability, high safety, enhanced cellular uptake in A549 cells, and PLGA shell thickness dependent transfection ability, in order to exert the therapeutic effect of siRNA in lung cancer, vectors must be able to penetrate into tumor tissue. In tumor tissue, the continuous proliferation of tumor cells will lead to an increase in density of solid tumors. Furthermore, in solid tumors, crucial stromal cells, such as tumor-associated fibroblast cells (TAFs), are found in almost all solid tumors, and they can further increase the density of solid tumors. The physical barrier formed by tumor cells and TAFs will prevent the deep tumor penetration of nanocarriers [31]. Therefore, the tumor spheroid penetration behavior of HNPs with different coating thickness was further investigated. To simulate solid tumors more realistically, 3T3 cells were selected as cell models of TAFs to form stroma, and they were added and co-cultured with A549 cells to form 3D-cultured multicellular tumor spheroids (MCTS) with a diameter of approximately 200 μm.

As shown in Fig. 7A, the tumor permeability of different nanocarriers was observed *via* CLSM. Semi-quantitative analysis was conducted on the drug penetration area at the center of spheroids (Section at a depth of 100 μm), and the results are expressed as percentage of the penetration area to the total tumor area. First of all, based on the cytotoxicity results, to ensure high cell viability of both Lpx and HNPs, tumor permeability was investigated at a lower siRNA concentration (50 nM). The results demonstrated that all the fluorescence intensity of different HNPs was higher than that of Lipo2000 and Lpx ($p < 0.01$), but there was no significant difference in tumor permeability between different HNPs ($p > 0.05$) (Fig. 7B). There are researches proved that tumor permeability was influenced by the flexibility and rigidity of nanocarriers, and liposomes with moderate rigidity had the best tumor permeability [28]. In our study, the PLGA shell undoubtedly increased the rigidity of Lpx. Therefore, the increase in tumor permeability may be due to the increase in rigidity of Lpx. In addition, according to a report, the movement distance of neutral nanoparticles (± 10 mV) was three times that of charged analogs, and they distributed more homogeneously within tissue [32]. Another study showed that compared to positively charged liposomes, liposomes with near neutral charges exhibited stronger tumor permeability [33]. Therefore, in our study, compared to highly positively charged Lpx, besides the increased rigidity, the near neutral charge of HNPs was also beneficial for tumor permeability. Furthermore, based on the results of cellular uptake in A549 cells, the high tumor permeability of HNPs may also related to their higher uptake than that of Lpx within 4 h, while high cellular uptake increases the chance for nanoparticles to permeate into the deeper tumor.

To further explain why the coating strategy with PLGA can enhance the tumor permeability of Lpx, taking the optimized HNP1 as example and Lpx as control, the model for nanomedicine migration was performed to observe transcytosis [19]. In the first case, A549 cells that had pre-ingested the FAM siRNA-loaded Lpx or HNP1 (cell A) were added to the upper chamber of Transwell model, while blank A549 cells (cell B) was cultured on the lower chamber. As shown in Fig. 7C, after incubation for 4 h, green fluorescence was observed in cell B. In another case, there were A549 cells that had pre-ingested the FAM siRNA-loaded Lpx or HNP1 (cell B) in the lower chamber. Similarly, the originally blank cells in upper chamber (cell A) showed green fluorescence (Fig. 7D).

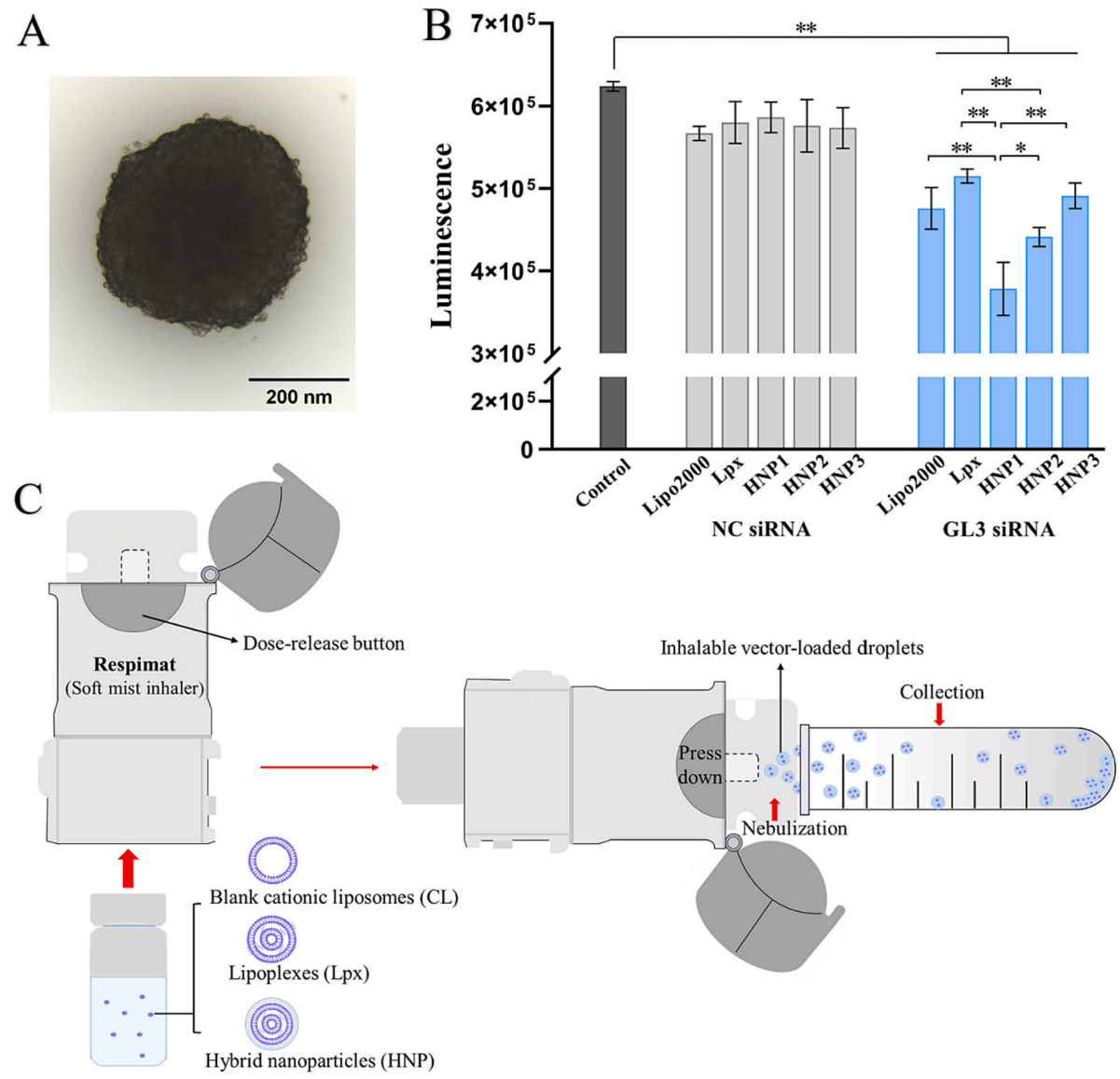

Fig. 8. (A) Image of 3D-cultured multicellular tumor spheroids (MCTS) of firefly luciferase A549-3T3 MCTS by light microscope. (B) Luminescence of firefly luciferase A549-3T3 MCTS after 48 h of transfection with scrambled (NC)/GL3 siRNA-loaded Lipo2000, Lpx, HNP1, HNP2, and HNP3. The concentration of scrambled/GL3 siRNA is 50 nM. The results of all NC and experimental groups were compared to that of the blank control group. $p < 0.05$ (*), $p < 0.01$ (**). (C) Schematic of nebulization process of the blank CL, Lpx, and HNPs *via* soft mist inhaler (Respimat®, Boehringer-Ingelheim, Germany). (D) Size and (E) PDI of blank CL and HNPs before and after nebulization. Results denote mean ± SD ($n = 3$).

These results of cell migration revealed that after vectors were internalized into endosomes, those vectors that did not escape from late endo/lysosomes and were not damaged by enzymes in acidic environment left the cells *via* lysosomal exocytosis [19,34]. The formation of ion pairs between DOTAP and the endosomal membrane will lead to structural damage of Lpx, which is beneficial for the release of siRNA and endosomal escape [16,20], but it is not conducive to transcytosis. Compared to Lpx, HNP with a PLGA rigid shell has enhanced stability, allowing some HNPs to maintain structural integrity in the endo/lysosomes, thus more HNPs are expelled from the cells to achieve the transfer of nanoparticles between adjacent cells in tumor spheroids. Furthermore, during the continuous entry of HNPs into the deeper tumor, as the PLGA shell ruptures, positively charged Lpx is exposed. Thus, charge reversal may be achieved within the tumor. The positive surface charge of nanomedicine is conducive to promoting adsorption-mediated transcytosis [31].

3.9. In vitro gene silencing in tumor spheroids

After proving that HNP1 with the thinnest PLGA shell has excellent transfection efficiency in 2D-cultured cells and the PLGA shell effectively increases the tumor permeability of Lpx in 3D-cultured cells, further study was conducted to test the potential application of HNPs in lung cancer therapy. To simulate the transfection of siRNA vectors in cancer tissue, 3D-cultured tumor spheroids of firefly luciferase A549-3T3 cells were constructed (Fig. 8A). Subsequently, gene silencing of Lipo2000, Lpx, and HNPs with different coating thickness in tumor spheroids were investigated. As shown in Fig. 8B, no significant difference in gene silencing between the blank control group and negative control groups was found ($p > 0.05$), indicating specific siRNA effects could be safely determined in 3D lung cancer cell models. Surprisingly, the complexity of solid tumors can hinder the penetration of nanoparticles into the depth of tumors, leading to significant differences in the results of gene silencing between 2D and 3D cell models, while the low tumor permeability of Lpx resulted in its lowest gene silencing in 3D-cultured tumor spheroids. In contrast, the coating strategy with PLGA increased the tumor permeability of Lpx, resulting in significantly higher gene silencing of HNP1 and HNP2 compared to Lpx ($p < 0.01$), but there was no significant difference in gene silencing between Lpx and HNP3 ($p > 0.05$). Moreover, among different HNPs, HNP1 showed the strongest gene silencing ($p < 0.05$), and its gene silencing was higher than that of Lipo2000 ($p < 0.01$). When the transfection efficiency of blank control group was set at 0%, the transfection efficiency of Lipo2000, Lpx, HNP1, HNP2, and HNP3 were 23.70 ± 3.31%, 17.41 ± 1.11%, 39.33 ± 4.21%, 29.23 ± 1.52%, and 21.25 ± 2.02%, respectively. These results verify our hypothesis again: HNP1 with the thinnest PLGA shell is stable enough in mucus and BALF to protect siRNA while it is prone to rupture in lysosome, leading to sufficient exposure of the lipid core, thereby inducing endosomal escape, and ultimately exhibiting the strongest gene silencing. To sum up, HNP1 is a promising non-viral vector of siRNA to enhance lung cancer therapy *via* pulmonary delivery.

3.10. Physical stability during nebulization

For pulmonary siRNA delivery, the vector must be appropriately inhaled by patients so as to better deposit in the lung. Inhalation delivery method is critical because it might affect physical stability of nanoparticle-based drug delivery systems, efficacy of inhalation, and even patient compliance [11]. Soft mist inhalers (SMIs) utilize mechanical power to form inhalable mists of drug solution. SMIs allow for a slower release of aerosol compared to traditional inhalers, resulting in a weaker destructive effect on drugs [35]. Currently, the Respimat® is the only commercially available SMI [35,36]. Thus, after demonstrating HNPs exhibited the potential application in lung cancer therapy, further study was conducted to investigate whether HNPs are suitable for inhalation using nebulizer. Respimat® was selected to nebulize suspensions of CL, Lpx, HNP1, HNP2, and HNP3 (Fig. 8C). The changes in particle size and PDI of different nanoparticles after nebulization were used to determine their physical stability. As shown in Fig. 8D, the particle size of CL, HNP1, and HNP2 increased slightly after nebulization (~10 nm). As shown in Fig. 8E, although the PDI of CL, HNP1, and HNP2 increased after nebulization, they were all <0.26, indicating particle sizes were still uniform. The particle size and PDI of HNP3 remained unchanged, possibly the thicker PLGA shell could better counteract dispersing force during nebulization. Contrarily, after siRNA and CL combined to form Lpx, Lpx continued to fuse with each other in cartridge, leading to a sharp increase in particle size and PDI after nebulization (Micrometer scale). This study demonstrated that compared to Lpx, HNPs showed superior physical stability during nebulization *via* SMIs.

3.11. Storage stability

Based on the above studies, HNP1 was the optimal choice. Thus, storage stability of HNP1 was further studied within 4 weeks. Due to fusion effect, Lpx exhibited strong aggregation (Micrometer scale) after 1 h, while the particle size of HNP1 had no significant change within 4 weeks ($p > 0.05$) and the PDI was <0.25, indicating the coating strategy with PLGA effectively enhanced the storage stability of Lpx (Fig.S3).

4. Conclusion

In this study, to overcome the hurdles of pulmonary siRNA delivery for lung tumor therapy, we demonstrated that coating cationic liposomes (CL) with biodegradable PLGA as the shell can form hybrid nanoparticles (HNPs) *via* microfluidic method, which as non-viral vectors can not only improve stability of siRNA in mucus and BALF, but also improve safety of CL by covering the positive charge, with enhanced mucus penetration and cellular uptake attributed to the increased rigidity of HNPs and the neutral surface. HNP1 with the thinnest PLGA coating and balanced stability showed the best gene silencing efficiency, which was comparable to that of Lpx and Lipofectamine 2000. Moreover, compared to CL and Lpx, HNPs remarkably enhanced tumor permeability in 3D-cultured tumor spheroids. In conclusion, this study demonstrated that HNP1 designed here can not only be used as promising non-viral vectors for enhanced lung cancer therapy *via* pulmonary siRNA delivery, it can also be used as siRNA carriers for other lung related diseases therapy with tunable rigidity, high transfection efficiency and good safety profile.

CRediT authorship contribution statement

Hezhi Wang: Writing – original draft, Software, Methodology, Investigation, Formal analysis, Data curation, Conceptualization. **Ye Yuan:** Methodology, Investigation, Formal analysis. **Lu Qin:** Methodology, Investigation. **Mengmeng Yue:** Methodology, Investigation. **Jingwen Xue:** Methodology, Investigation. **Zhixiang Cui:** Software, Data curation. **Xuanguang Zhan:** Methodology, Investigation. **Jiayi Gai:** Methodology, Investigation. **Xin Zhang:** Software, Project administration. **Jian Guan:** Software, Resources. **Shirui Mao:** Writing – review & editing, Supervision, Resources, Project administration, Funding acquisition, Formal analysis, Data curation, Conceptualization.

Declaration of competing interest

The authors declare no conflicts of interest.

Data availability

Data will be made available on request.

Acknowledgement

This project is financially supported by the National Key Research and Development Program of China (No. 2020YFE0201700) and the Key Research Funding of Education Department of Liaoning Province (2022).

Appendix A. Supplementary data

Supplementary data to this article can be found online at https://doi.org/10.1016/j.jconrel.2024.01.029.

References

[1] M. Roman, I. Baraibar, I. Lopez, E. Nadal, C. Rolfo, S. Vicent, I. Gil-Bazo, KRAS oncogene in non-small cell lung cancer: clinical perspectives on the treatment of an old target, Mol. Cancer 17 (2018) 33.
[2] D.I. Suster, M. Mino-Kenudson, Molecular pathology of primary non-small cell lung Cancer, Arch. Med. Res. 51 (2020) 784–798.
[3] V. Kumar, S. Yadavilli, R. Kannan, A review on RNAi therapy for NSCLC: opportunities and challenges, Wiley Interdiscip, Rev.-Nanomed. Nanobiotechnol. 13 (2021) e1677.
[4] X. Liang, D. Li, S. Leng, X. Zhu, RNA-based pharmacotherapy for tumors: from bench to clinic and back, Biomed. Pharmacother. 125 (2020) 109997.
[5] G. Ozcan, B. Ozpolat, R.L. Coleman, A.K. Sood, G. Lopez-Berestein, Preclinical and clinical development of siRNA-based therapeutics, Adv. Drug Deliv. Rev. 87 (2015) 108–119.
[6] Y.Z. Dong, D.J. Siegwart, D.G. Anderson, Strategies, design, and chemistry in siRNA delivery systems, Adv. Drug Deliv. Rev. 144 (2019) 133–147.
[7] P. Khan, J.A. Siddiqui, I. Lakshmanan, A.K. Ganti, R. Salgia, M. Jain, S.K. Batra, M. W. Nasser, RNA-based therapies: a cog in the wheel of lung cancer defense, Mol. Cancer 20 (2021) 54.
[8] N.R. Labiris, M.B. Dolovich, Pulmonary drug delivery. art I: physiological factors affecting therapeutic effectiveness of aerosolized medications, Br. J. Clin. Pharmacol. 56 (2003) 588–599.
[9] M. Ibrahim, L. Garcia-Contreras, Mechanisms of absorption and elimination of drugs administered by inhalation, Ther. Deliv. 4 (2013) 1027–1045.
[10] Q. Liu, J. Guan, L. Qin, X. Zhang, S. Mao, Physicochemical properties affecting the fate of nanoparticles in pulmonary drug delivery, Drug Discov. Today 25 (2020) 150–159.
[11] H. Wang, L. Qin, X. Zhang, J. Guan, S. Mao, Mechanisms and challenges of nanocarriers as non-viral vectors of therapeutic genes for enhanced pulmonary delivery, J. Control. Release 352 (2022) 970–993.
[12] M. Schlich, R. Palomba, G. Costabile, S. Mizrahy, M. Pannuzzo, D. Peer, P. Decuzzi, Cytosolic delivery of nucleic acids: the case of ionizable lipid nanoparticles, Bioeng Transl Med 6 (2021) e10213.
[13] M. Zoulikha, Q. Xiao, G.F. Boafo, M.A. Sallam, Z. Chen, W. He, Pulmonary delivery of siRNA against acute lung injury/acute respiratory distress syndrome, Acta Pharm. Sin. B 12 (2022) 600–620.
[14] S. Simoes, A. Filipe, H. Faneca, M. Mano, N. Penacho, N. Duzgunes, M.P. de Lima, Cationic liposomes for gene delivery, Expert Opin. Drug Deliv. 2 (2005) 237–254.
[15] J. Zhao, L. Qin, R. Song, J. Su, Y. Yuan, X. Zhang, S. Mao, Elucidating inhaled liposome surface charge on its interaction with biological barriers in the lung, Eur. J. Pharm. Biopharm. 172 (2022) 101–111.
[16] Y. Xia, J. Tian, X. Chen, Effect of surface properties on liposomal siRNA delivery, Biomaterials 79 (2016) 56–68.
[17] C. Conte, F. Mastrotto, V. Taresco, A. Tchoryk, F. Quaglia, S. Stolnik, C. Alexander, Enhanced uptake in 2D-and 3D-lung cancer cell models of redox responsive PEGylated nanoparticles with sensitivity to reducing extra- and intracellular environments, J. Control. Release 277 (2018) 126–141.
[18] Q. Liu, J. Xue, X. Zhang, J. Chai, L. Qin, J. Guan, X. Zhang, S. Mao, The influence of a biomimetic pulmonary surfactant modification on the in vivo fate of nanoparticles in the lung, Acta Biomater. 147 (2022) 391–402.
[19] Y. Liu, Y. Huo, L. Yao, Y. Xu, F. Meng, H. Li, K. Sun, G. Zhou, D.S. Kohane, K. Tao, Transcytosis of nanomedicine for tumor penetration, Nano Lett. 19 (2019) 8010–8020.
[20] B.-K. Kim, G.-B. Hwang, Y.-B. Seu, J.-S. Choi, K.S. Jin, K.-O. Doh, DOTAP/DOPE ratio and cell type determine transfection efficiency with DOTAP-liposomes, Biochim. Biophys. Acta 2015 (1848) 1996–2001.
[21] Z.C. Deng, G.T. Kalin, D.L. Shi, V.V. Kalinichenko, Nanoparticle delivery systems with cell-specific targeting for pulmonary diseases, Am. J. Respir. Cell Mol. Biol. 64 (2021) 292–307.
[22] S. Garg, G. Heuck, S. Ip, E. Ramsay, Microfluidics: a transformational tool for nanomedicine development and production, J. Drug Target. 24 (2016) 821–835.
[23] C.B. Roces, G. Lou, N. Jain, S. Abraham, A. Thomas, G.W. Halbert, Y. Perrie, Manufacturing considerations for the development of lipid nanoparticles using microfluidics, Pharmaceutics 12 (2020) 1095.
[24] M.H.Y. Cheng, J. Leung, Y. Zhang, C. Strong, G. Basha, A. Momeni, Y. Chen, E. Jan, A. Abdolahzadeh, X. Wang, J.A.A. Kulkarni, D. Witzigmann, P.R.R. Cullis, Induction of bleb structures in lipid nanoparticle formulations of mRNA leads to improved transfection potency, Adv. Mater. 35 (2023) e2303370.
[25] B.S. Schuster, J.S. Suk, G.F. Woodworth, J. Hanes, Nanoparticle diffusion in respiratory mucus from humans without lung disease, Biomaterials 34 (2013) 3439–3446.
[26] J. Sun, L. Zhang, J. Wang, Q. Feng, D. Liu, Q. Yin, D. Xu, Y. Wei, B. Ding, X. Shi, X. Jiang, Tunable rigidity of (polymeric Core)-(lipid Shell) nanoparticles for regulated cellular uptake, Adv. Mater. 27 (2015) 1402–1407.
[27] T. Stern, I. Kaner, N.L. Zer, H. Shoval, D. Dror, Z. Manevitch, L. Chai, Y. Brill-Karniely, O. Benny, Rigidity of polymer micelles affects interactions with tumor cells, J. Control. Release 257 (2017) 40–50.
[28] H. Wu, M. Yu, Y. Miao, S. He, Z. Dai, W. Song, Y. Liu, S. Song, E. Ahmad, D. Wang, Y. Gan, Cholesterol-tuned liposomal membrane rigidity directs tumor penetration and anti-tumor effect, Acta Pharm. Sin. B 9 (2019) 858–870.
[29] J. Zhao, J. Su, L. Qin, X. Zhang, S. Mao, Exploring the influence of inhaled liposome membrane fluidity on its interaction with pulmonary physiological barriers, Biomater. Sci. 8 (2020) 6786–6797.
[30] E.M.M. Manders, F.J. Verbeek, J.A. Aten, Measurement of co-localization of objects in dual-colour confocal images, J. Microsc. 169 (1993) 375–382.
[31] Z. Li, X. Shan, Z. Chen, N. Gao, W. Zeng, X. Zeng, L. Mei, Applications of surface modification Technologies in Nanomedicine for deep tumor penetration, Adv. Sci. 8 (2021) 2002589.
[32] M.J. Ernsting, M. Murakami, A. Roy, S.-D. Li, Factors controlling the pharmacokinetics, biodistribution and intratumoral penetration of nanoparticles, J. Control. Release 172 (2013) 782–794.
[33] T. Nomura, N. Koreeda, F. Yamashita, Y. Takakura, M. Hashida, Effect of particle size and charge on the disposition of lipid carriers after intratumoral injection into tissue-isolated tumors, Pharm. Res. 15 (1998) 128–132.
[34] S. Buratta, B. Tancini, K. Sagini, F. Delo, E. Chiaradia, L. Urbanelli, C. Emiliani, Lysosomal exocytosis, exosome release and secretory autophagy: the Autophagic- and Endo-lysosomal systems go extracellular, Int. J. Mol. Sci. 21 (2020) 2576.
[35] V. Komalla, C.Y.J. Wong, I. Sibum, B. Muellinger, W. Nijdam, V. Chaugule, J. Soria, H.X. Ong, N.A. Buchmann, D. Traini, Advances in soft mist inhalers, Expert Opin. Drug Deliv. 20 (2023) 1055–1070.
[36] R. Dhand, J. Eicher, M. Haensel, I. Jost, M. Meisenheimer, H. Wachtel, Improving usability and maintaining performance: human-factor and aerosol-performance studies evaluating the new reusable Respimat inhaler, Int. J. Chron. Obstruct. Pulmon. Dis. 14 (2019) 509–523.